HHS Public Access

Author manuscript

NMR Biomed. Author manuscript; available in PMC 2017 July 01.

Published in final edited form as:

NMR Biomed. 2016 July ; 29(7): 978–984. doi:10.1002/nbm.3557.

Functional and Anatomical Characterization of Brown Adipose Tissue in Heart Failure with Blood Oxygen Level Dependent Magnetic Resonance

Marcello Panagia, MD, DPhil[*,†,§,#], **Yin-Ching Iris Chen, PhD**[§,#], **Howard H Chen, PhD**[§], **Laura Ernande, MD, PhD**[†,‖], **Chan Chen, MD, PhD**[¶], **Wei Chao, MD, PhD**[¶], **Kenneth Kwong, PhD**[§], **Marielle Scherrer-Crosbie, MD, PhD**[†], and **David E. Sosnovik, MD**[†,§]

[*]Cardiology Section, Boston Medical Center, Boston, MA

[†]Cardiology Division, Massachusetts General Hospital, Boston, MA

[§]Martinos Center for Biomedical Imaging, Department of Radiology, Massachusetts General Hospital, Boston MA

[‖]DHU Ageing-Thorax-Vessel-Blood, Hôpital Henri Mondor, AP-HP, Créteil, France

[¶]Department of Anesthesia, Critical Care and Pain Medicine, Massachusetts General Hospital, Harvard Medical School

Abstract

Recent studies have suggested that brown adipose tissue (BAT) plays an important role in obesity, insulin resistance and heart failure. The characterization of BAT *in vivo*, however, has been challenging. No technique to comprehensively image BAT anatomy and function has been described. Moreover, the impact on BAT of the neuroendocrine activation seen in heart failure has only recently begun to be evaluated *in vivo.* The aim of this study was to use MRI to characterize the impact of heart failure on the morphology and function of BAT.

Mice subjected to permanent ligation of the left coronary artery were imaged with MRI 6 weeks later. T2 weighted MRI of BAT volume and blood oxygen level dependent MRI of BAT function were performed. T2* maps of BAT were obtained at multiple time points before and after administration of the β3 adrenergic agonist CL-316,243 (CL). Blood flow to BAT was studied after CL injection using the flow alternating inversion (FAIR) recovery approach. Excised BAT tissue was analysed for lipid droplet content and for uncoupling protein (UCP1) mRNA expression.

BAT volume was significantly lower in heart failure (51 ± 1 mm^3 vs 65 ± 3 mm^3; $p<0.05$), and characterized by a reduction in lipid globules and a 4-fold increase in UCP1 mRNA ($p<0.05$). CL injection increased BAT T2* in healthy animals but not in mice with heart failure (24±4% vs 6±2%; $p<0.01$), consistent with an increase in flow in control BAT. This was confirmed by a significant difference in the FAIR response in BAT in control and heart failure mice.

Correspondence: David E. Sosnovik, MD, Martinos Center for Biomedical Imaging, Massachusetts General Hospital and Harvard Medical School, 149 13th St, Charlestown, MA 02129, VOICE: (617) 724-3407, sosnovik@nmr.mgh.harvard.edu.

[#]These authors have contributed equally to this work.

There are no relevant relationships with industry to report.

Heart failure results in the chronic activation of BAT, decreased BAT lipid stores, decreased BAT volume and it is associated with a marked decrease in its ability to respond to acute physiological stimuli. This may have important implications for substrate utilization and overall metabolic homeostasis in heart failure.

Keywords

Brown Adipose Tissue; BOLD; Heart Failure; MRI

Introduction

The recent identification of discrete depots of brown adipose tissue (BAT) in adults [1–5] has stimulated interest in the role of BAT in human physiology. Traditionally, BAT was thought to be primarily responsible for non-shivering thermogenesis in rodents and newborn humans [6]. The energy stored in the mitochondrial proton gradient in BAT is dissipated by uncoupling proteins (UCP1) in the mitochondrial membrane [7, 8] generating heat. More recently, however, there have been suggestions for an expanded role of BAT in whole body energy regulation, insulin sensitivity and heart failure, though the precise mechanisms for these roles are still being investigated [9–12].

The factors leading to the activation of BAT in adults remain poorly understood. In addition to its activation by cold via sympathetic stimulation through β_3 adrenergic receptors [13, 14], recent work has suggested that natriuretic peptides released from the heart can also activate BAT, though the exact mechanism involved in this activation remains unclear [11, 15, 16]. Moreover, a recent study demonstrates that BAT can modulate cardiomyocyte injury in catecholamine induced cardiomyopathy suggesting that there is cross–talk between BAT and the heart in mice [12]. We hypothesized here that the properties of BAT would be significantly changed in heart failure, and produce both anatomical and functional changes detectable with magnetic resonance.

Recent studies have shown that it is possible to accurately measure BAT volume using MRI, by taking advantage of its unique water/fat composition compared to adjacent tissues [17–19]. Moreover, functional MRI techniques, such as blood-oxygen-level-dependent (BOLD) contrast, can be used to assess the metabolic activity of BAT independent of substrate selection [19–21]. While deoxyhemoglobin produced by oxidative metabolism of active tissue reduces the BOLD (T2*) signal, the increase in flow seen during local tissue activation increases the local BOLD signal and T2*. The observed T2* value is a balance of these opposing effects [22–25]. We hypothesized that the addition of spin labeling to measure flow would allow changes in the BOLD signal to be more accurately interpreted. Here we used BOLD MRI and flow sensitive alternating inversion recovery (FAIR) to image BAT in normal mice and mice with heart failure, at rest and after β_3 adrenergic stimulation. To the best of our knowledge, this is the first description of functional MRI to characterize the properties of BAT in heart failure.

Experimental

Mouse Model

Twelve week old female C57BL/6 mice were purchased from Jackson Laboratories (Bar Harbor, Maine). A myocardial infarction (MI) was induced by coronary ligation, as previously described [26]. In brief, permanent occlusion of the left coronary artery was performed with an 8–0 suture, and myocardial ischemia confirmed by tissue blanching and ECG monitoring. Animals were allowed to recover and imaged 6 weeks after the surgery at 18 weeks of age (n=5). The 6-week time point was chosen to allow the heart time to remodel fully after the myocardial infarct. The control mice, which were age and sex matched, were also imaged at 18 weeks (n=5).

Magnetic Resonance Imaging

MRI studies were peformed on a 9.4T scanner (Biospec, Bruker, Billerica, MA) with a 4-element phased array receive coil (Bruker, Billerica, MA) placed over the interscapular area. All MRI scans were acquired with respiratory gating to minimize respiratory artifact (Small Animal Instruments, Inc, Stony Brook, NY). Ambient temperature inside the imaging bore was maintained at 30°C via an optical-controlled hot air heating system (Small Animal Instruments, Inc, Stony Brook, NY). Animals were anesthetized with sodium pentobarbital throughout the imaging session (initial dose 50–75 mg/kg, ip, booster dose 20 mg/kg ip every 30 min, begining one hour after the initial dose). Heart rate and respiratory rate were continuously monitored during the imaging session.

T2 weighted RARE (rapid acquisition of refocused echoes) was used for the anatomical delineation of BAT [19]. Parameters included: Field of view (FOV) of 2.56 cm, slice thickness of 1 mm, matrix of 128×128 (in-plane resolution of 0.2 mm by 0.2 mm), 10 slices, repetition time (TR) 2000 ms, effective echo time (TE) 37 ms, RARE factor of 8, 4 averages. BOLD MRI of BAT was performed with a multi-echo gradient echo sequence with the identical FOV and resolution and the following parameters: TR 500 ms, initial TE 2.6 ms, total of 8 echoes, echo spacing 1.4 ms, flip angle 45°, averages 1. Sequential imaging was performed at 20 consecutive time points scanning a range of approximately 40 min. To acutely activate BAT, an intravenous bolus of CL-316,243, a beta3 agonist, (1mg/kg IV dissolved in saline) was administered at the 10^{th} time point, resulting in an equal number of T2* values at baseline and following β_3 adrenergic stimulation.

Blood flow to BAT was estimated using the FAIR approach[27, 28], and measured before and after the BOLD protocol. T1 values in BAT were acquired with an ECG-gated Look-Locker sequence, using slice selective and non-selective adiabatic inversion recovery pulses. Single slice images were obtained with 20 degree excitation pulses and 50 segmentations with TR 3.73 ms, TE 1.5 ms and a scan repetition time of 3000 ms. The 20° flip angle used was based on prior simulations using a transmit surface coil and likely led to some perturbation of magnetization recovery with the volume coil used in this study. This could have led to an underestimation of T1 in both the control and heart failure mice. T1 values from selective and non-selective inversion recovery sequences were fitted from 50 inversion delay times (TI) (initial delay of 10 ms and 22 ms increments) using MATLAB (lsqcurvefit).

Following MRI of BAT, cine MRI of the heart was performed to measure LV volume and function. Gradient echo cine images were acquired in the short axis of the left ventricle using cardiorespiratory gating (SA Instruments, Stonybrook, NY) as previously described [26, 29] with the following settings: FOV 2.5 × 2.5cm^2, slice thickness 1mm, matrix, 192 × 192, flip angle 30°, 20 frames per R-R interval, TE 1.6 ms, 4 averages.

Image Analysis

Image analysis was performed using Osirix (v5.8.5) and Freesurfer (v5.3.0). BAT was identified on the T2 weighted RARE images based on its location posterior to the interscapular white adipose tissue, its characteristic bi-lobed shape, and signal hypointensity relative to white adipose (Figure 1). Regions of interest (ROIs) were manually drawn around BAT tissue in each 2D slice and then summed using a Simpson's approach over the entire 3D volume.

ROIs delineating BAT were also manually drawn in each slice for the T2* calculation. The mean T2* value in each ROI was calculated using a mono-exponential decay model available in the Osirix image processing software. At each time point, the T2* values in all 10 slices were averaged to yield a single T2* value for that time point. The T2* values at each time point were then normalized to the baseline T2* value (time point 1), as previously described [30, 31]. ROIs were also drawn in an adjacent segment of skeletal muscle and T2* was calculated as described above. T1 relaxation curves were derived at a single slice location in the center of the BAT tissue using the same ROI that was used for the T2* calculation. The difference in T1 (ΔT1) of the BAT tissue between the acquisitions with non-selective ($T1_{NS}$) and slice selective ($T1_{SS}$) inversion pre-pulses was calculated, and used as a measure of flow (larger 3T1 = higher flow).

Flow (F) within the tissue was defined [32] as $F=(\Delta T1*\lambda)/(T1_{Blood}*T1_{SS})$, where λ is the blood-tissue partition coefficient. Vessels supplying blood to BAT were not clearly identifiable in most of the FAIR images and absolute flow, which requires $T1_{Blood}$, was thus not calculated. No significant differences were seen in $T1_{SS}$ between the control and heart failure mice, either pre or post CL-injection. Assuming that no differences in λ and $T1_{Blood}$ were present between the control and heart failure mice under a given condition (pre or post CL-injection), the relative flow (RF) for that state was given by: $RF= (\Delta T1_{Failure})/(\Delta T1_{Control})$.

Left ventricular ejection fraction was measured by cine MRI. End diastolic and end systolic volumes were calculated by manually tracing the endocardial border of the left ventricle at end diastole and end systole in each short axis slice. The volumes in each short axis slice were summed using the Simpson's method. Ejection fraction (EF) was calculated as (end diastolic volume – end systolic volume)/end diastolic volume.

Histology and Quantification of UCP1

Mice were euthanized, and their brown adipose tissue was carefully dissected and sectioned into 5μm thick paraffin-embedded sections. Staining of the BAT was performed using hematoxylin & eosin. UCP1 levels in BAT were quantified by measuring mRNA. The BAT was dissected and snap frozen in liquid nitrogen. RNA was extracted using Trizol

(Invitrogen, Carlsbad, CA), and cDNA for UCP1 was synthesized using MMLV-RT (Promega, Madison, WI). Real-time amplification of transcripts was performed using a Mastercycler ep Realplex (Eppendorf, Hamburg, Germany). The relative expression of mRNA was normalized to levels of 18S RNA. Primer pairs were used to detect transcripts encoding for UCP1 [33].

Statistical Analysis

Unpaired t-tests were used to compare control and heart failure groups. Two-tailed probability values are reported and statistical significance is defined as $p<0.05$. Values are reported as mean ± standard deviation (SD). All statistical analyses were performed using Prism v6.0 (Graphpad Software Inc. LaJolla, CA).

Results

BAT Volume in Heart Failure

BAT could be easily identified in all mice based on its location, bi-lobed shape and signal hypointensity relative to overlying white adipose tissue (Figure 1). Infarct size in the mice subjected to coronary ligation varied, reflecting changes in the location of the ligation. A representative image of the heart of an infarcted mouse is shown in Figure 1, where the left ventricle is dilated with a large aneurysm. BAT volume in mice with an EF >65% was $65\pm3mm^3$ versus $51\pm1mm^3$ in mice with an EF <45% ($p<0.05$, $n = 5$ in both groups)

BAT Activation in Heart Failure

Heart rate and respiratory rates were continuously monitored during the imaging session and were not significantly different between the groups. Baseline BAT T2* in control mice averaged 7.2±0.9 ms, which was similar to T2* in skeletal muscle (8.4±1.0 ms). To facilitate comparison between the control and heart failure groups, T2* values were normalized in each animal to the T2* at the first time point for that animal. Normalized T2* values at each time point were then averaged across the group, as previously described [30]. Peak T2* in BAT after CL administration (Figure 2, arrow, Figure 3) was 1.2× fold higher than baseline in the control animals but did not significantly change in the heart failure animals ($p < 0.01$). In fact, T2* of BAT in mice with heart failure showed little, if any, increase in response to CL injection. The increase in control T2* was transient, forming a sharp spike lasting 4–6 minutes. In both control and heart failure BAT, the steady state T2* value after CL injection trended to a lower value than pre-injection.

No significant response to CL injection was seen in the skeletal muscle of either control mice or mice with heart failure (Figure 2, Figure 3). The peak-trough difference in BAT T2* normalized for baseline T2* was significantly higher in control mice than the mice with heart failure (0.26±0.12 vs 0.10±0.06; $p<0.05$) (Figure 3) but no significant differences in normalized peak-trough T2* were seen in skeletal muscle between the groups (Figure 3). Analysis of the FAIR data revealed that the relative increase in blood flow in BAT post CL injection was 2.1 fold ($p < 0.05$) greater in control versus heart failure animals (Figure 4). Blood flow to BAT prior to CL injection was not significantly different between the groups (Figure 4).

BAT Histology and UCP1 mRNA Content in Heart Failure

Hematoxylin and eosin staining of BAT in control animals showed brown adipocytes containing multilocular lipid globules that were markedly decreased in size and number in the mice subjected to coronary ligation and heart failure (Figure 5), suggesting an increase in lipolysis in these mice. UCP1 mRNA in BAT (normalized to 18S RNA) was 4× higher in the heart failure mice ($p < 0.05$).

Discussion

The impact of heart failure on BAT remains unknown. Here we demonstrate that significant anatomical, functional, and molecular differences exist between BAT of healthy mice and mice with impaired cardiac function. We demonstrate that post-MI, BAT volume is lower, lipid droplet content is lower and BAT UCP1 mRNA is higher. In addition, the flow and BOLD responses of BAT to β_3 adrenergic stimulation are blunted in heart failure. These results suggest that baseline BAT activity is increased in heart failure, but that its functional reserve is decreased, and are in accordance with prior *in vitro* studies suggesting that the neuroendocrine signals activated in heart failure could potentially modulate metabolic activity in BAT [11, 15, 16, 34]. Future study will be needed to determine whether the relationships between serum levels of catecholamines, natriuretic peptides and metrics of BAT activation by MRI are linear or non-linear. Further studies will also be needed to determine whether the activation of BAT in heart failure is adaptive or maladaptive, but recent work suggests that the presence of BAT may protect the heart against injury [12].

One of the major obstacles impeding a fuller understanding of the role of BAT has been the inability to noninvasively characterize its anatomy and function. Positron emission tomography (PET) of fluordeoxyglucose (^{18}FDG) has been used over the last decade [1, 3, 35, 36], however, ^{18}FDG is a functional readout of BAT metabolism, and its ability to accurately resolve the anatomical dimensions of BAT is limited. In addition, ^{18}FDG relies on imaging active BAT and does not account for BAT's ability to utilize other oxidizable substrates, such as free fatty acids and triglycerides. An alternative approach has used contrast ultrasound to quantify changes in blood flow to BAT during activation in mice [33, 37] and in humans [38]. The advantage of this approach lies in its high throughput and wide availability; however, ultrasound lacks the tomographic properties and soft tissue contrast obtainable with MRI.

Recent work in normal animals has shown that T2 weighted MRI can accurately delineate BAT based on its inherent magnetic properties [19, 21]. BOLD MRI has also been shown to detect changes in BAT activity following sympathetic stimulation [19]. Here, to the best of our knowledge, for the first time, we use functional MRI to characterize the response of BAT to impaired cardiac function. Further, while BOLD and FAIR have been used extensively in the heart to measure tissue perfusion with endogenous contrast [39–42], they have not hitherto been used together to image BAT. Here we use these techniques in combination to better characterize the nature of the BOLD response in BAT in mice with heart failure.

The central finding of this study is that BAT structure and function is altered in heart failure. This is shown by decreased BAT volume by MRI, a reduction in the size and number of lipid

droplets in BAT by histology and increased UCP1 levels in the BAT of mice with impaired cardiac function. Moreover, BAT function was altered in animals with heart failure as the BOLD response to acute sympathetic stimulation was significantly blunted. It should be noted that in the heart failure group, some of the mice remained relatively well compensated despite a significant reduction in EF whereas other mice showed overt signs of decompensated heart failure such as pleural effusions. Further study will be needed to determine whether the properties of BAT differ significantly in those with compensated (stage B) and decompensated (stage C) heart failure.

BOLD MRI has been extensively used to study brain activity [43]. Metabolic activation leads to increased oxygen extraction and increased production of deoxyhemoglobin, which is paramagnetic and decreases T2*. However, the increased production of deoxyhemoglobin is offset, and strongly exceeded, by the increase in local blood flow seen during metabolic activation [43, 44]. BOLD contrast is thus dominated by the impact of flow, which causes T2* to increase during metabolic activation. The blunted functional (T2*) response to CL injection seen in BAT of heart failure mice thus represents an inability to increase local blood flow. This was confirmed using FAIR, which showed a significantly lower flow response in the heart failure mice. This could be due to an inability to augment stroke volume or due to the down-regulation of BAT beta-adrenergic receptors in heart failure in response to chronically elevated circulating catecholamine levels [45].

The acute stimulation of BAT with noradrenaline has been shown to increase blood flow for at least 30 minutes or longer compared to baseline [46]. The FAIR imaging in our study, which was performed approximately 20 minutes after CL injection, showed a persistent relative increase in blood flow in control BAT compared to heart failure BAT at that time. However, the spike in BAT T2* following CL injection was more transient (4–6 minutes) and actually settled towards a lower steady state value than pre-injection. This suggests that the initial response of BAT to β_3 adrenergic is strongly dominated by an increase in flow. After a lag period of several minutes, however, the increase in deoxyhemoglobin production matches and even exceeds the increase in flow and returns T2* to baseline. This observation is consistent with the role of BAT in thermogenesis though its implications to heart failure require further study.

At baseline, the absolute T2* values in BAT in the mice with coronary ligation and heart failure were lower than controls, but this trend did not reach significance. Likewise, no significant difference was seen in baseline flow to BAT between the two groups. This suggests that baseline oxygen extraction and deoxyhemoglobin production in BAT were higher in the mice with heart failure, although the impact of this effect on baseline T2* did not reach significance. T2* values in skeletal muscle directly adjacent to BAT were used in this study to control for differences in cardiac output and edema between animals. No differences in skeletal muscle T2* were seen between the control and heart failure mice. In addition, consistent with prior studies [21], no change in the BOLD signal in skeletal muscle was seen in response to CL injection. The observed changes in T2* in BAT were thus specific and directly reflected local rather than global changes in flow and oxidative metabolism.

Therefore, we conclude that heart failure results in a decrease in BAT volume and lipid droplet size as well as an increase in UCP1 mRNA, all suggestive of increased BAT activity. In addition, heart failure is associated with a blunted vascular response to acute BAT activation by adrenergic agonists. MRI is able to image BAT volume and the functional activity of BAT using BOLD and FAIR. Further information on BAT metabolism could be obtained by incorporating spectroscopy of either ^{31}P or hyperpolorized ^{13}C metabolites into the acquisition. In addition, integrated MR-PET scanners are now widely available and would allow imaging of ^{18}FDG, or other relevant metabolites, to be integrated with the MRI readout. MRI is thus likely to play an increasingly important role in the evaluation of BAT and the development of strategies to modulate its activity.

Supplementary Material

Refer to Web version on PubMed Central for supplementary material.

Acknowledgments

Funding: This research was supported by the following National Institutes of Health grants: K08 HL123744-03 (M.P.) R01 HL093038 (D.E.S.), R01HL112831 (D.E.S.), P41RR14075 to the Martinos Center for Biomedical Imaging, R01 GM080906 (W.C.), R01 GM097259 (W.C.), SPARK grant from MGH (M.S.C) and DK R21 092909 (M.S.C).

Abbreviations

BAT	brown adipose tissue
BOLD	blood oxygen dependent level
CL	CL 316,243
EF	left ventricular ejection fraction
^{18}F-FDG	^{18}F-fluorodeoxyglucose
FAIR	flow sensitive alternating inversion recovery
FSE	fast spin echo
H&E	hematoxylin and eosin
IP	intraperitoneal
IV	intravenous
MI	myocardial infarction
MRI	magnetic resonance imaging
PET	positron emission tomography
ROI	region of interest
TR	repetition time

TE	echo time
UCP1	uncoupling protein 1

References

1. Virtanen KA, Lidell ME, Orava J, Heglind M, Westergren R, Niemi T, Taittonen M, Laine J, Savisto NJ, Enerbäck S. Functional brown adipose tissue in healthy adults. N Engl J Med. 2009; 360:1518–1525. [PubMed: 19357407]
2. Yeung HWD, Grewal RK, Gonen M, Schöder H, Larson SM. Patterns of (18)F-FDG uptake in adipose tissue and muscle: a potential source of false-positives for PET. Journal of Nuclear Medicine. 2003; 44:1789–1796. [PubMed: 14602861]
3. Hany TF, Gharehpapagh E, Kamel EM, Buck A, Himms-Hagen J, Schulthess von GK. Brown adipose tissue: a factor to consider in symmetrical tracer uptake in the neck and upper chest region. Eur J Nucl Med Mol Imaging. 2002; 29:1393–1398. [PubMed: 12271425]
4. Cypess AM, Lehman S, Williams G, Tal I, Rodman D, Goldfine AB, Kuo FC, Palmer EL, Tseng Y-H, Doria A, Kolodny GM, Kahn CR. Identification and Importance of Brown Adipose Tissue in Adult Humans. N Engl J Med. 2009; 360:1509–1517. [PubMed: 19357406]
5. van Marken Lichtenbelt WD, Vanhommerig JW, Smulders NM, Drossaerts JMAFL, Kemerink GJ, Bouvy ND, Schrauwen P, Teule GJJ. Cold-activated brown adipose tissue in healthy men. N Engl J Med. 2009; 360:1500–1508. [PubMed: 19357405]
6. Rothwell NJ, Stock MJ. A role for brown adipose tissue in diet-induced thermogenesis. Nature. 1979; 281:31–35. [PubMed: 551265]
7. Nedergaard J, Golozoubova V, Matthias A, Asadi A, Jacobsson A, Cannon B. UCP1: the only protein able to mediate adaptive non-shivering thermogenesis and metabolic inefficiency. Biochimica et Biophysica Acta (BBA)-Bioenergetics. 2001; 1504:82–106. [PubMed: 11239487]
8. Rial E, González-Barroso MM, Fleury C, Bouillaud F. The structure and function of the brown fat uncoupling protein UCP1: current status. Biofactors. 1998; 8:209–219. [PubMed: 9914821]
9. Vijgen GHEJ, Bouvy ND, Teule GJJ, Brans B, Schrauwen P, van Marken Lichtenbelt WD. Brown adipose tissue in morbidly obese subjects. PLoS ONE. 2011; 6:e17247. [PubMed: 21390318]
10. Stanford KIK, Middelbeek RJWR, Townsend KLK, An DD, Nygaard EBE, Hitchcox KMK, Markan KRK, Nakano KK, Hirshman MFM, Tseng Y-HY, Goodyear LJL. Brown adipose tissue regulates glucose homeostasis and insulin sensitivity. J Clin Invest. 2013; 123:215–223. [PubMed: 23221344]
11. Collins S. A heart-adipose tissue connection in the regulation of energy metabolism. Nature Reviews Endocrinology. 2014; 10:157–163.
12. Thoonen R, Ernande L, Cheng J, Nagasaka Y, Yao V, Miranda-Bezerra A, Chen C, Chao W, Panagia M, Sosnovik DE, Puppala D, Armoundas AA, Hindle A, Bloch KD, Buys ES, Scherrer-Crosbie M. Functional brown adipose tissue limits cardiomyocyte injury and adverse remodeling in catecholamine-induced cardiomyopathy. J Mol Cell Cardiol. 2015; 84:202–211. [PubMed: 25968336]
13. Mirbolooki MR, Upadhyay SK, Constantinescu CC, Pan M-L, Mukherjee J. Adrenergic pathway activation enhances brown adipose tissue metabolism: A [(18)F]FDG PET/CT study in mice. Nucl Med Biol. 2014; 41:10–16. [PubMed: 24090673]
14. Tam CS, Lecoultre V, Ravussin E. Brown adipose tissue: mechanisms and potential therapeutic targets. Circulation. 2012; 125:2782–2791. [PubMed: 22665886]
15. Collins S, Bordicchia M. Heart hormones fueling a fire in fat. Adipocyte. 2013; 2:104–108. [PubMed: 23805407]
16. Bordicchia M, Liu D, Amri E-Z, Ailhaud G, Dessì-Fulgheri P, Zhang C, Takahashi N, Sarzani R, Collins S. Cardiac natriuretic peptides act via p38 MAPK to induce the brown fat thermogenic program in mouse and human adipocytes. J Clin Invest. 2012; 122:1022–1036. [PubMed: 22307324]
17. Hu HH, Smith DL, Nayak KS, Goran MI, Nagy TR. Identification of brown adipose tissue in mice with fat-water IDEAL-MRI. J Magn Reson Imaging. 2010; 31:1195–1202. [PubMed: 20432356]

18. Branca RT, Warren WS. In vivo brown adipose tissue detection and characterization using water-lipid intermolecular zero-quantum coherences. Magn Reson Med. 2010; 65:313–319. [PubMed: 20939093]
19. Chen YI, Cypess AM, Sass CA, Brownell A-L, Jokivarsi KT, Kahn CR, Kwong KK. Anatomical and functional assessment of brown adipose tissue by magnetic resonance imaging. Obesity (Silver Spring). 2012; 20:1519–1526. [PubMed: 22343821]
20. Chen HH, Mekkaoui C, Cho H, Ngoy S, Marinelli B, Waterman P, Nahrendorf M, Liao R, Josephson L, Sosnovik DE. Fluorescence tomography of rapamycin-induced autophagy and cardioprotection in vivo. Circulation: Cardiovascular Imaging. 2013; 6:441–447. [PubMed: 23537953]
21. Khanna A, Branca RT. Detecting brown adipose tissue activity with BOLD MRI in mice. Magn Reson Med. 2012; 68:1285–1290. [PubMed: 22231619]
22. Detre JA, Leigh JS, Williams DS, Koretsky AP. Perfusion imaging. Magn Reson Med. 1992; 23:37–45. [PubMed: 1734182]
23. Turner R, Le Bihan D, Moonen CT, Despres D, Frank J. Echo-planar time course MRI of cat brain oxygenation changes. Magn Reson Med. 1991; 22:159–166. [PubMed: 1798390]
24. Thulborn KR, Waterton JC, Matthews PM, Radda GK. Oxygenation dependence of the transverse relaxation time of water protons in whole blood at high field. Biochim Biophys Acta. 1982; 714:265–270. [PubMed: 6275909]
25. Ogawa S, Lee TM, Nayak AS, Glynn P. Oxygenation-sensitive contrast in magnetic resonance image of rodent brain at high magnetic fields. Magn Reson Med. 1990; 14:68–78. [PubMed: 2161986]
26. Huang S, Chen HH, Yuan H, Dai G, Schuhle DT, Mekkaoui C, Ngoy S, Liao R, Caravan P, Josephson L, Sosnovik DE. Molecular MRI of acute necrosis with a novel DNA-binding gadolinium chelate: kinetics of cell death and clearance in infarcted myocardium. Circulation: Cardiovascular Imaging. 2011; 4:729–737. [PubMed: 21836081]
27. Kwong KK, Chesler DA, Weisskoff RM, Donahue KM, Davis TL, Ostergaard L, Campbell TA, Rosen BR. Mr perfusion studies witht1-weighted echo planar imaging. Magn Reson Med. 1995; 34:878–887. [PubMed: 8598815]
28. Look DC. Time Saving in Measurement of NMR and EPR Relaxation Times. Review of Scientific Instruments. 1970; 41:250.
29. Sosnovik DE, Garanger E, Aikawa E, Nahrendorf M, Figuiredo J-L, Dai G, Reynolds F, Rosenzweig A, Weissleder R, Josephson L. Molecular MRI of cardiomyocyte apoptosis with simultaneous delayed-enhancement MRI distinguishes apoptotic and necrotic myocytes in vivo: potential for midmyocardial salvage in acute ischemia. Circulation: Cardiovascular Imaging. 2009; 2:460–467. [PubMed: 19920044]
30. Partovi S, Schulte AC, Jacobi B, Klarhöfer M, Lumsden AB, Loebe M, Davies MG, Noon GP, Karmonik C, Zipp L, Bongartz G, Bilecen D. Blood oxygenation level-dependent (BOLD) MRI of human skeletal muscle at 1. 5 and 3 T. J Magn Reson Imaging. 2012; 35:1227–1232. [PubMed: 22246901]
31. Englund EK, Langham MC, Li C, Rodgers ZB, Floyd TF, Mohler ER, Wehrli FW. Combined measurement of perfusion, venous oxygen saturation, and skeletal muscle T2* during reactive hyperemia in the leg. J Cardiovasc Magn Reson. 2013; 15:70. [PubMed: 23958293]
32. Belle V, Kahler E, Waller C, Rommel E, Voll S, Hiller KH, Bauer WR, Haase A. In vivo quantitative mapping of cardiac perfusion in rats using a noninvasive MR spin-labeling method. J Magn Reson Imaging. 1998; 8:1240–1245. [PubMed: 9848735]
33. Baron DM, Clerte M, Brouckaert P, Raher MJ, Flynn AW, Zhang H, Carter EA, Picard MH, Bloch KD, Buys ES, Scherrer-Crosbie M. In vivo noninvasive characterization of brown adipose tissue blood flow by contrast ultrasound in mice. Circulation: Cardiovascular Imaging. 2012; 5:652–659. [PubMed: 22776888]
34. Wang TJ. The Natriuretic Peptides and Fat Metabolism. N Engl J Med. 2012; 367:377–378. [PubMed: 22830469]

35. Cypess AM, Chen Y-C, Sze C, Wang K, English J, Chan O, Holman AR, Tal I, Palmer MR, Kolodny GM, Kahn CR. Cold but not sympathomimetics activates human brown adipose tissue in vivo. Cell Metabolism. 2012; 109:10001–10005.

36. Orava J, Nuutila P, Lidell ME, Oikonen V, Noponen T, Viljanen T, Scheinin M, Taittonen M, Niemi T, Enerbäck S, Virtanen KA. Different Metabolic Responses of Human Brown Adipose Tissue to Activation by Cold and Insulin. Cell Metabolism. 2011; 14:272–279. [PubMed: 21803297]

37. Clerte M, Baron DM, Brouckaert P, Ernande L, Raher MJ, Flynn AW, Picard MH, Bloch KD, Buys ES, Scherrer-Crosbie M. Brown adipose tissue blood flow and mass in obesity: a contrast ultrasound study in mice. J Am Soc Echocardiogr. 2013; 26:1465–1473. [PubMed: 23993691]

38. Flynn A, Li Q, Panagia M, Abdelbaky A, MacNabb M, Samir A, Cypess AM, Weyman AE, Tawakol A, Scherrer-Crosbie M. Contrast-Enhanced Ultrasound: A Novel Noninvasive, Nonionizing Method for the Detection of Brown Adipose Tissue in Humans. J Am Soc Echocardiogr. 2015; 28:1247–1254. [PubMed: 26255029]

39. Friedrich MG, Niendorf T, Schulz-Menger J, Gross CM, Dietz R. Blood oxygen level-dependent magnetic resonance imaging in patients with stress-induced angina. Circulation. 2003; 108:2219–2223. [PubMed: 14557359]

40. Friedrich MG, Karamitsos TD. Oxygenation-sensitive cardiovascular magnetic resonance. J Cardiovasc Magn Reson. 2013; 15:43. [PubMed: 23706167]

41. Gutjahr FT, Kampf T, Winter P, Meyer CB, Williams T, Jakob PM, Bauer WR, Ziener CH, Helluy X. Quantification of perfusion in murine myocardium: A retrospectively triggered T1 -based ASL method using model-based reconstruction. Magn Reson Med. 2014

42. Tsaftaris SA, Zhou X, Tang R, Li D, Dharmakumar R. Detecting myocardial ischemia at rest with cardiac phase-resolved blood oxygen level-dependent cardiovascular magnetic resonance. Circulation: Cardiovascular Imaging. 2013; 6:311–319. [PubMed: 23258476]

43. Kwong KK, Belliveau JW, Chesler DA, Goldberg IE, Weisskoff RM, Poncelet BP, Kennedy DN, Hoppel BE, Cohen MS, Turner R. Dynamic magnetic resonance imaging of human brain activity during primary sensory stimulation. Proc Natl Acad Sci U S A. 1992; 89:5675–5679. [PubMed: 1608978]

44. Hoppel BE, Weisskoff RM, Thulborn KR, Moore JB, Kwong KK, Rosen BR. Measurement of regional blood oxygenation and cerebral hemodynamics. Magn Reson Med. 1993; 30:715–723. [PubMed: 8139453]

45. Bengtsson T, Cannon B, Nedergaard J. Differential adrenergic regulation of the gene expression of the beta-adrenoceptor subtypes beta1, beta2 and beta3 in brown adipocytes. Biochem J. 2000; 347(Pt 3):643–651. [PubMed: 10769166]

46. Nagashima T, Ohinata H, Kuroshima A. Involvement of nitric oxide in noradrenaline-induced increase in blood flow through brown adipose tissue. Life Sci. 1994; 54:17–25. [PubMed: 8255165]

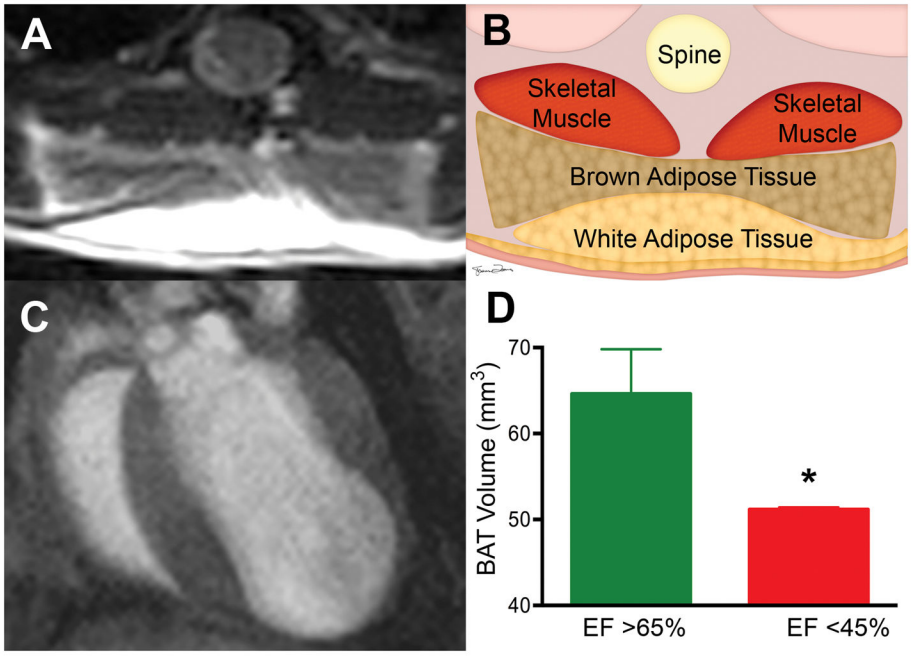

Figure 1. Impact of Ejection Fraction on BAT Volume

(A) T2 weighted RARE image allowing BAT to be clearly differentiated from surrounding WAT and skeletal muscle. (B) Schematic of the tissues shown in panel A: BAT forms a bi-lobed structure between the more superficial WAT and deeper skeletal muscle. (C) End diastolic frame of the heart of a mouse 6 weeks after left coronary artery ligation. The left ventricular apex is thin and aneurysmal. BAT volume was significantly lower in animals with a low ejection fraction resulting from coronary ligation (D) (*$p<0.05$). Error bars represent SD. *EF*= Ejection Fraction; *BAT* = Brown Adipose Tissue ; *WAT* = White Adipose Tissue; *RARE* = Rapid acquisition of refocused echoes.

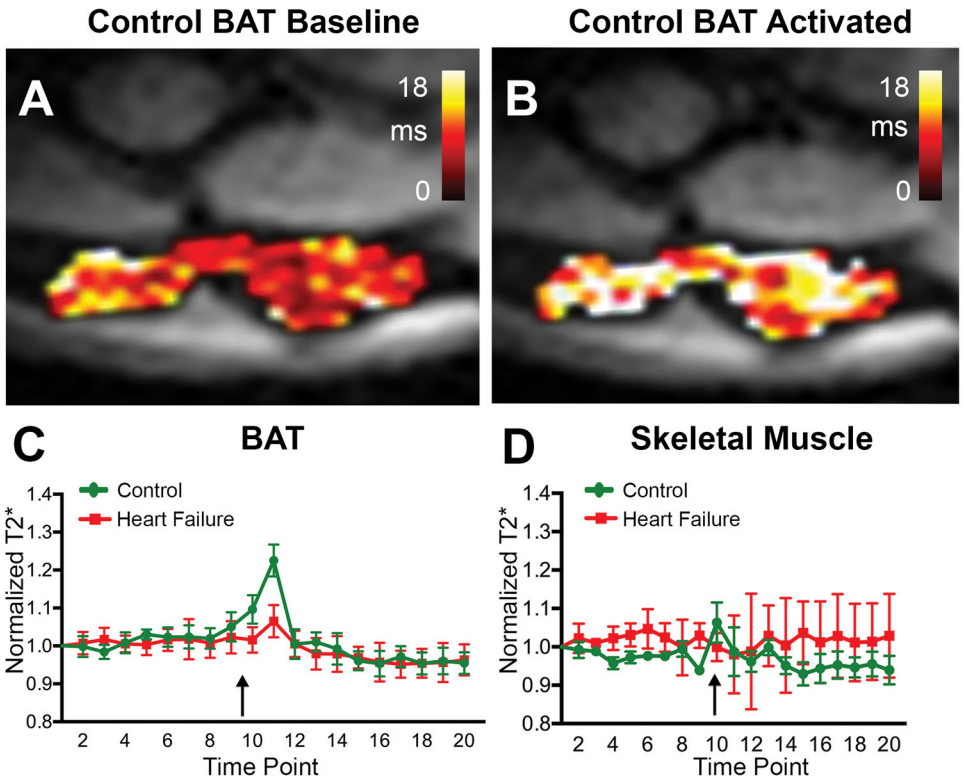

Figure 2. BOLD response of BAT is blunted in heart failure

Normalized T2* in BAT and skeletal muscle in mice with heart failure and aged matched control mice. (A, B) T2* map in a control mouse at baseline (A) and after activation with CL (B). (C) T2* in the control mice (n=5) increased significantly after CL injection, while in the heart failure mice (n=5) this response was significantly blunted. The spike in BAT T2* was transient and in both sets of mice T2* trended to a lower steady state value post-CL injection than pre-injection. The black arrow marks the injection of 1mg/Kg IV of CL. (D) CL injection did not significantly alter T2* in the skeletal muscle adjacent to BAT in either the control or heart failure mice. *BAT* = Brown Adipose Tissue, *CL* = CL 316,243.

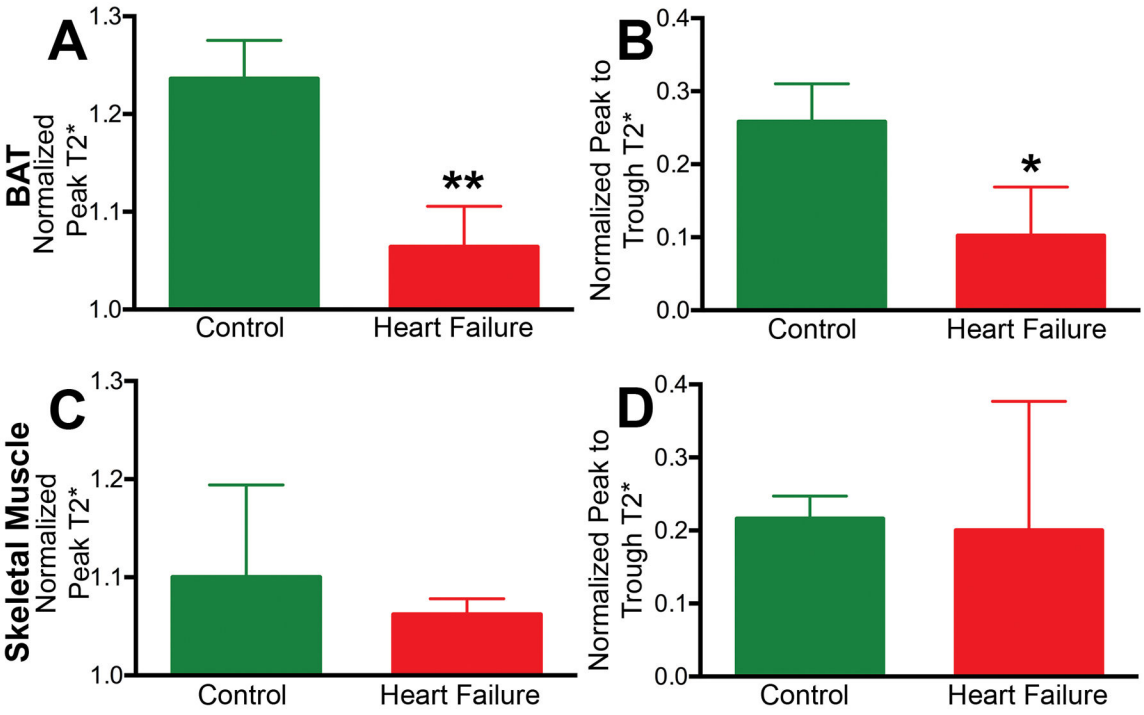

Figure 3. Metabolic response in BAT differs from skeletal muscle

In BAT, significant differences were seen between control and heart failure mice in (A) normalized peak T2* after CL injection and (B) peak to trough T2*. (C, D) In skeletal muscle, these parameters did not differ significantly between the control and heart failure mice. (* $p < 0.05$, ** $p < 0.01$). *BAT* = Brown Adipose Tissue, *CL* = CL 316,243.

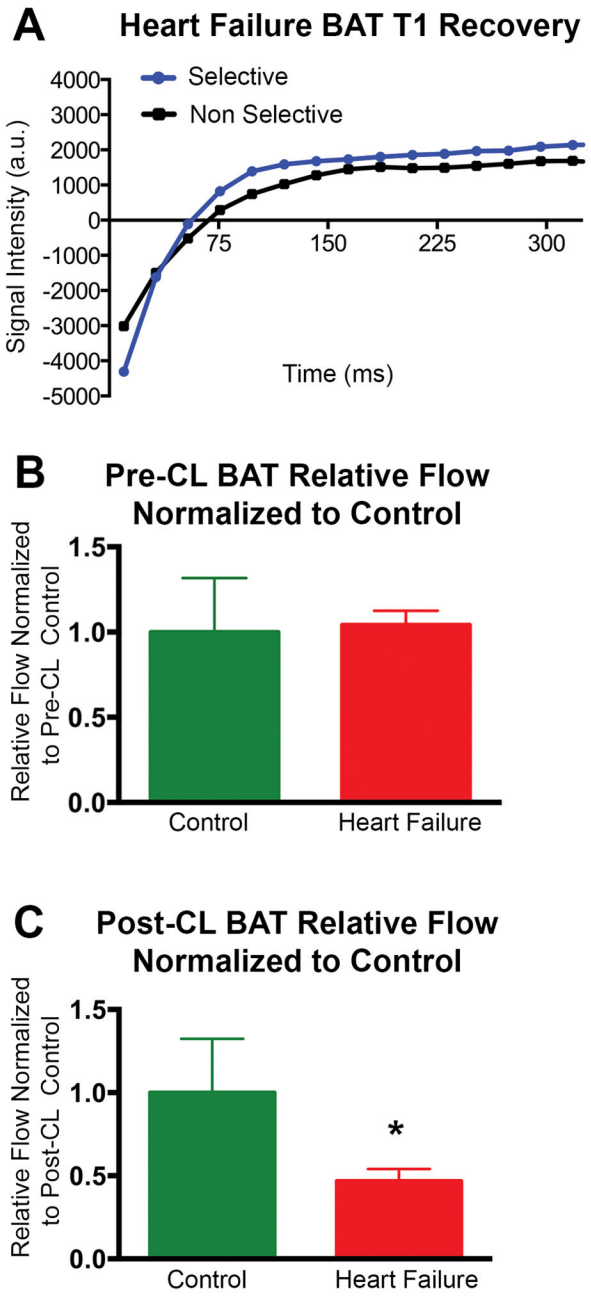

Figure 4.

(A) T1 Recovery curves after slice-selective and non-selective inversion pre-pulses in the BAT of a mouse with heart failure. The difference in the two curves reflects relative flow. (B) Relative flow (normalized to pre-CL control) in control and heart failure BAT showing no difference between the groups prior to CL injection. (C) Relative flow (normalized to post-CL control) in control and heart failure BAT showing a significant blunting to the increase in relative flow in response to CL injection in heart failure BAT ($p < 0.05$) *BAT* = Brown Adipose Tissue, *CL* = CL 316,243.

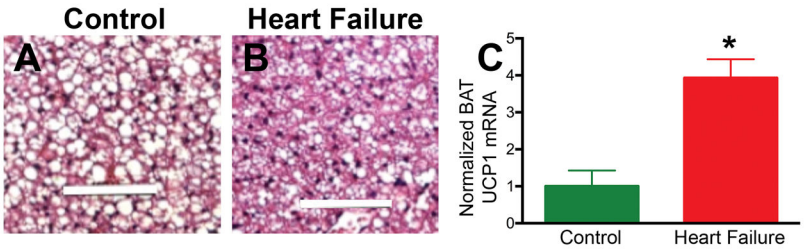

Figure 5. Biochemical changes in BAT in heart failure

Hematoxylin and eosin staining of BAT in a control mouse (A) and a mouse with heart failure (B). The size of the lipid globules (white areas on the slide) inside the adipocytes is decreased in heart failure, suggesting increased lipolysis. (C) A significant increase in UCP1 mRNA (* $p < 0.05$) is seen in the BAT of mice with heart failure, suggesting increased BAT activity. *UCP1*= Uncoupling Protein 1; White bar 100μm, *BAT* = Brown Adipose Tissue.